Surface plasmon resonance microscopy: achieving a quantitative optical response

Alexander W. Peterson,[a)] Michael Halter, Anne L. Plant, and John T. Elliott

Biosystems and Biomaterials Division, National Institute of Standards and Technology, 100 Bureau Dr., Gaithersburg, MD 20899, USA

Surface plasmon resonance (SPR) imaging allows real-time label-free imaging based on index of refraction, and changes in index of refraction at an interface. Optical parameter analysis is achieved by application of the Fresnel model to SPR data typically taken by an instrument in a prism based configuration. We carry out SPR imaging on a microscope by launching light into a sample, and collecting reflected light through a high numerical aperture microscope objective. The SPR microscope enables spatial resolution that approaches the diffraction limit, and has a dynamic range that allows detection of subnanometer to submicrometer changes in thickness of biological material at a surface. However, unambiguous quantitative interpretation of SPR changes using the microscope system could not be achieved using the Fresnel model because of polarization dependent attenuation and optical aberration that occurs in the high numerical aperture objective. To overcome this problem, we demonstrate a model to correct for polarization diattenuation and optical aberrations in the SPR data, and develop a procedure to calibrate reflectivity to index of refraction values. The calibration and correction strategy for quantitative analysis was validated by comparing the known indices of refraction of bulk materials with corrected SPR data interpreted with the Fresnel model. Subsequently, we applied our SPR microscopy method to evaluate the index of refraction for a series of polymer microspheres in aqueous media and validated the quality of the measurement with quantitative phase microscopy.

I. INTRODUCTION

Surface plasmon resonance (SPR) is a label-free surface sensitive technique that can be used to determine the refractive index of a material at a thin metal surface.[1] Typically, the technique is used to perform kinetic analysis of binding interactions for DNA olgionucleiotides [2] or proteins [3] by tracking the change in the angle of minimum reflectance over time as more material binds or dissociates from the

[a)] Author to whom correspondence should be addressed. Electronic mail: alexander.peterson@nist.gov.

surface. It has been shown that the SPR reflectivity profile, i.e., the angle-dependent change in reflectivity, can be modeled and fit by the Fresnel equations, which allows determination of thickness, mass, and/or index of refraction of the surface bound material.[4] Unlike critical angle refractometer measurements which are sensitive only to the bulk media, an SPR measured index of refraction is inherently sensitive to material within the evanescent field generated at the surface.

SPR imaging (SPRI) is an application of SPR that provides the ability to monitor spatial changes in reflectivity at an angle that is close to the resonance minimum.[5-9] Using a prism to disperse and couple the incident light into a surface at a fixed angle, the technique has been used to monitor the kinetics of protein or oligonucleotide binding in a 2-dimensional array format over areas of several square millimeters.[10, 11] SPRI has also been applied to studies in cell biology, where it can be used to provide spatial measurement of cell-secreted proteins over time,[12] and visualization of cellular adhesion and migration events that are not easily observed with transmission microscopy techniques.[13] At a fixed angle of incident light, such as that achieved with a prism, the reflectivity values of the SPR image can be converted into mass or index of refraction values. However, more accurate measurements of the index of refraction could be achieved if Fresnel modeling of the reflectivity measurements over a range of incident angles could be performed on the image data.

SPR microscopy using a high numerical aperture (NA) objective has been demonstrated.[14, 15] The approach has the potential advantage that the surface sensitive SPR measurements can be easily combined with other microscopic imaging modes such as bright field and fluorescence microscopy. Although these previous studies have demonstrated imaging of reflectivity changes at a surface, quantitative interpretation of the index of refraction of imaged features using Fresnel equations has not been achieved. Achieving accurate measures of index of refraction with SPR microscopy requires rectifying the Fresnel model to compensate for the optical aberrations in the objective lens, and applying the corrections required to compensate for the polarization apodization in a high NA objective, which creates a nonlinear, angle-dependent decay in light intensity.

Here, we describe SPR microscopy (also referred to as SPRI) using a high NA objective and a digital light projector (DLP) as the excitation light source.[16] The DLP allows specific selection of the angle, or a range of angles, of the linearly polarized incident light that is provided through the high NA objective. Using a modified microscope platform, we can image both the back focal plane (BFP) and the image plane. The BFP can be imaged to provide the SPR angular response from a sample that is illuminated with light at a range of incident angles; the SPR reflectivity image can be collected from the image plane using light at a single angle of incidence.

The SPR angular response in the BFP indicates an angle dependent polarization apodization which complicates direct fitting of the angle-dependent SPR signal with Fresnel equations. Using these empirical data, we apply a correction to the SPR data, and fit the data with the Fresnel model to achieve an accurate interpretation of index of refraction. We use this method to evaluate bulk materials and compare our measurements with known index values. Using both the angle-dependent SPR response from the BFP and the SPRI reflectivity data from the image plane, we demonstrate how to characterize the linear response range for the SPRI system, and provide a conversion of reflectivity to index of refraction values for each pixel in the image. Subsequently, we use this system calibration to measure the index of refraction of porous polymer microspheres, and compare these values with an independent measurement by quantitative phase microscopy. As a result of this effort, we identified a microsphere with an index of refraction near that of hydrated proteins that can serve as both a spatial and intensity calibrant for SPRI of biological samples.

II. MATERIALS AND METHODS

A. SPR microscopy

For SPR microscopy, we performed SPR on an inverted microscope (Olympus IX-70, Center Valley, PA)[17] with a high numerical aperture objective lens (100x, 1.65 NA, Olympus) by launching incident light into the lens and collecting reflected light from the sample on the microscope stage. The illumination source is a digital light projector

(DLP; Dell 3300MP; Dell, Round Rock, TX) that is controlled with a laptop computer using Power Point (Microsoft, Redmond, WA) to fully illuminate the back focal plane (BFP) with white light, or to transmit only some of the light in the form of specific crescent shapes. The white light is transmitted through a transparent window on the internal DLP filter wheel, which allows subsequent selection of wavelength of incident light with an external filter. The projector lens was removed and replaced with a 4X objective (Edmund Optics, Barrington, NJ). The focused light was collimated with an achromatic lens (f=60 mm) and directed through a bandpass filter (centered at 590 nm; full-width-half-maximum (FWHM) = 10 nm; Thorlabs, Newton, NJ), and a rotatable linear polarizer (Thorlabs). This polarized monochromatic light is directed into a customized tube lens (f=100 mm), through a filter cube mounted with a pellicle beam splitter (Thorlabs), and onto the BFP of the high numerical aperture objective lens. The incident light was projected onto the BFP by reducing the spot size to 1/3 through the choice of a collimating lens and a tube lens with appropriate focal lengths and distance between them according to the thin lens formula.[18] Samples were prepared on coverslips (No. 0, Olympus), which were coated with a thin film of gold (described in Section II B), and which were coupled to the objective with refractive index (n) matching fluid, n = 1.78 (Cargille Laboratories, Cedar Grove, NJ). Incident light couples to the plasmons in the gold film with a fraction of the p-polarized light being reflected or absorbed depending on the angle of incidence and the material at the surface. The reflected SPR image is directed out the microscope body, through a series of lenses (effectively a Bertrand lens) that can be inserted or removed from the beam path so as to select for either the image plane or back focal plane, and onto a 12-bit Coolsnap FX charged-coupled device (CCD) camera (Roper Scientific, Tucson, AZ). Images were collected using Micro-Manager (www.micro-manager.org) open source microscopy software.

B. Substrate Preparation

Specialized coverslips (18 mm diameter, n = 1.78, Olympus) were acid washed with 7:3 volume ratio H_2SO_4:H_2O_2, rinsed with 18 MΩ distilled water, rinsed with ethanol, dried, and then coated with ≈1 nm chromium and ≈45 nm gold (99.99% purity by mass) by magnetron sputtering using an Edwards Auto 306 vacuum system (Edwards, Wilmington, MA) at $1x10^{-7}$ mbar. For microsphere based experiments, a static fluidic chamber made out of polydimethylsiloxane (PDMS) was assembled on top of the coverslip and the bare gold surface under distilled water was used as the substrate and media.

C. SPR BFP Collection and Correction

To image the SPR signal on the BFP, the DLP is set to project non-patterned white light to fully illuminate the BFP field. The excitation wavelength is selected by the 590 nm bandpass filter. The lens assembly before the camera is set to project the BFP onto the camera CCD. A homogeneous sample, for example, a gold coated coverslip in a water-filled chamber, is mounted via coupling fluid on the objective. One image is taken with the linear polarizer oriented in the direction of the *x*-axis of the image. This is labeled the p-polarized light image, and the minimum SPR reflectivity is visible at the periphery of the BFP in the *x*-axis but not in the *y*-axis. A second s-polarized light image is taken by rotating the linear polarizer 90°, whereupon the SPR minimum is observed along the *y*-axis and not the *x*-axis.

An image of the BFP is obtained when the sample on the microscope stage is fully illuminated with projected light that is p-polarized. The intensity of reflected light as a function of distance from the center of the image to the periphery is selected using a line scan in image analysis software. The distance in pixels is converted to angles at which incidence light impinges on the sample according to the Abbe sine condition,[19] $d = A \sin \theta$, where d is the distance from center to periphery of the BFP in pixels, A is a constant, and θ is the angle of incidence in degrees (Supplementary Material, Fig. S1). The value of A is determined by measuring a known angle of incidence. Here, it can be seen that for water (n = 1.33) on a coverslip (n = 1.78), the critical angle, i.e., the angle at which total internal reflection occurs, can be determined from the inflection point of the SPR reflectivity profile to be 48.49 degrees. The same angle conversion is performed for an s-polarized line scan taken of the same length.

The angle-dependent intensities of p-polarized light are then divided by the corresponding s-polarized light intensities. Dividing the p- polarized by the s- polarized light provides a normalized value for reflectivity, and also normalizes reflectivity for spatial inhomogeneity in the incident light, as only p-polarized light interacts with the surface plasmons while the s-polarized light remains proportional to the incident light. However, due to aberrations caused by the high NA objective, the s-polarized light no longer remains directly proportional to the incident light at high incident angles.[20] To correct for this apodization, the p/s intensity profile is measured with an *x*-axis line scan and a *y*-axis line scan as described above using an optically thick gold coated glass, so as not to generate a surface plasmon, and this p/s intensity profile provides an apodization function. Dividing the original SPR p/s line scan by this apodization function yields the corrected SPR angle scan with appropriately normalized reflectivity units, which can be subsequently fit by the Fresnel model using literature values for the optical constants of the layers involved

(glass/gold/media).[21-23] To apply the correction as a mathematical equation, this apodization profile can be expressed an exponential function of the form $Ae^{(x/c)} + y_1$, where x is the incident angle in degrees and the other values are fitted constants (A, c, and y_1).

D. Shaping the Projected Incident Light

Prior to imaging the sample on the microscope stage, the angle and shape of the incident light are optimized by imaging the BFP. A sample is mounted on the stage and coupled to the objective lens with index matching fluid, and the DLP is used to fully illuminate the BFP with p-polarized light. The SPR minimum near the periphery of the image of the BFP can be viewed in the ocular objective or the CCD camera. A software generated image projected from the DLP is then used to illuminate only a thin crescent-shaped beam of light of ≈40 arc degrees to impinge on the sample, and the resulting reflected light is viewed at the BFP. The crescent-shape light is initially placed near where the SPR minimum was visualized when the BFP was fully illuminated. Switching the optics from viewing the BFP to allow viewing of the image plane in the microscope ocular or the CCD camera, the position of the crescent-shaped light is then finely tuned by using the software to translate the crescent-shaped image in the x-direction until the SPR intensity value in the image plane is minimized. The corrected minimum reflectivity observed for the wavelength and gold thickness used in this imaging system is ≈0.05. The position of the crescent shape is then adjusted to be slightly left of the SPR minimum (i.e. closer to the center of the objective), to achieve a reflectivity of ≈0.1, which ensures that the subsequent SPR imaging response will be in the linear response range.[24] Therefore, the use of the BFP image allows one to obtain the average SPR-dependent reflectivity of the sample as a function of incident angle of light. By employing this routine on a bulk sample of homogeneous refractive index, one can use the average reflectivity value from the image plane to accurately determine the incident angle of the illuminating light for the microscope system. For measurements of distilled water on bare gold, we determined that for this imaging system, the incident angle is calculated to be ≈56.5°.

E. SPR Image Collection and Correction

For each SPR image collected from the image plane, both a p- and s-polarized image are taken by rotating the linear polarizer 90° while using the crescent-shaped illumination. The p-polarized image is divided by the s-polarized image to reduce the spatial artifacts in the SPR image due to spatial inhomogeneity in the incident light.[16] The p/s intensities for each pixel are then divided by the apodization correction factor, which is a function of the

calculated incident angle. The result is an image with normalized and corrected reflectivity units. For incident light of 590 nm launched into the sample at a 56.5° incident angle, the apodization correction factor for this imaging system is 2.4. For subsequent analysis and comparison, the images are further modified to convert the reflectivity units into Δ-reflectivity (ΔR) by using $\Delta R = R_1 - R_0$ where R_1 is the normalized reflectivity unit of the sample and R_0 is the average reflectivity of the SPR image of water, which we use as a calibration material. In the case of the polymer microsphere images, a background region of interest is used to calculate R_0. All image analysis was performed using ImageJ software with additional custom script programming. Angle-dependent SPR data were analyzed using stock and custom code written in MATLAB (Mathworks, Natick, MA).

F. Index of Refraction Measurement of Bulk Materials by Critical Angle Refractometry

Critical angle reflectance measurements were made to provide independent refractive index measurements to compare and validate SPR measurements. The critical angle reflectance data were collected on a custom-built variable-angle instrument designed for SPR measurements and described previously.[25] The critical angle reflectivity curves were performed at 590 nm for 18 MΩ distilled water, phosphate-buffered saline (PBS) pH 7.2 solution (Life Technologies, Grand Island, NY), ethanol (100 %, The Warner-Graham Company, Cockeysville, MD), and a polymerized piece of polydimethylsiloxane (PDMS, Sylgard 184, Dow Corning, Midland, MI). The initial calibration for the angle of incidence was performed by using the published values for the refractive index of water, $n = 1.333$.[22] Each critical angle reflectance data set was fit to a two-layer Fresnel model,[26] using literature values for the optical constants of the prism,[21] to calculate the refractive index of the bulk material (Supplementary Material, Fig. S2). The error (standard deviation) in fitting the individual critical angle scan was 1×10^{-6} refractive index units. The error between replicates was 1×10^{-4} refractive index units.

G. Index of Refraction Measurement of Bulk Materials by SPRI

The materials described above for use as reference and test materials, water, PBS buffer, ethanol and PDMS, were each placed in a static fluid chamber on top of a gold coated coverslip. SPR reflectivity as a function of incident angle was measured by imaging the fully illuminated BFP as described above. Water was used as the reference material for determining the angle of incidence in the imaging system since the refractive index of water, n=1.333, is a highly reliable value. The angle of incidence was fine-tuned by fitting the Fresnel model to the angle dependent SPR reflectivity of water using literature values for the optical constants of the other optical layers (glass/gold).[21-23] The

indices of refraction for the remaining materials were determined by fitting the Fresnel model to the angle-dependent SPR intensities using the same optical constants and the angles of incidence determined from the SPR reflectivity of the water reference.

To assure accuracy of the refractive index determined from Fresnel modeling of the SPR intensities, the angle at which reflectivity is a minimum was determined by fitting a parabola to the angle-dependent resonance profile for each material. Using water as a reference, the absolute angle of minimum reflectivity was converted to a relative angle ($\Delta\theta_{min}$) by subtracting the angle of minimum reflectivity for the substance from the value for water. The Fresnel model, using the optical parameters fit to water as described above, was used to simulate a SPR refractive index response from n = 1.333 to 1.430. The angle minimum (θ_{min}) was extracted from each SPR angle simulation and converted to relative angle ($\Delta\theta_{min}$) to water. The response of relative angle minimum ($\Delta\theta_{min}$) versus refractive index (n) serves as the comparison between the SPR measured materials and the Fresnel model simulation.

For comparison of refractive index with the Δ-reflectivity values measured from the SPR reflectivity images, a simulation is performed with the Fresnel model originally fit to the water sample. Keeping all other parameters fixed, the refractive index of the media is incremented from n = 1.333 to n = 1.430 and at each increment the reflectivity value of the model SPR curve from a 56.5 degree incident angle is plotted as a function of the refractive index. The resulting plot is ΔR as a function of refractive index, and serves as comparison of the SPRI measured materials and Fresnel model simulation.

H. Index of Refraction Measurement of Polymer Microspheres by SPRI

Polymer microspheres of various materials and sizes were obtained as listed here: silica microspheres (n = 1.42, diameter 6.1 μm; Bangs Laboratories, Inc., Fishers, IN), poly(methyl methacrylate) (PMMA) microspheres (n = 1.48, diameter 63 μm to 75 μm; Cospheric, Santa Barbara, CA), gelatin-agarose microspheres (diameter 45 μm to 165 μm; Sigma-Aldrich, St. Louis, MO), and Sephacryl S-300 microspheres (diameter 25 μm to 75 μm; GE Healthcare Biosciences, Pittsburgh, PA). In most cases, ≈100 μL of stock bead suspension was diluted 1/10 in distilled water. This dilution was centrifuged and then resuspended with 1 mL nanopure distilled water, repeated twice. An aliquot of the distilled water-bead suspension was then added to a fluid chamber mounted on a gold coated substrate at room temperature. If the microspheres were shipped dry, the first step was to add an aliquot of beads to a microfuge tube and resuspend in 1 mL distilled water.

SPR images of the beads were collected at an angle of incident light of 56.5° and at a wavelength of 590 nm, and image processing was performed as described above. The reflectivity values in the images were then converted to ΔR units normalized to water. All microspheres are in water media and therefore the relative intensities, ΔR, of the background region of the SPR images is considered to be ≈ 0.00. Reflectivity was measured over the width of the microspheres and pixels with the largest reflectivity values were reported as ΔR_{max}. The reported standard deviation is from 6-10 measurements of each polymer material. As described in Section II G to show the relationship between Δ-reflectivity and refractive index, the ΔR_{max} values for each microsphere are converted into refractive index values with associated standard deviation values.

I. Quantitative Phase Imaging

Quantitative phase imaging (QPI) was performed according to the transport of intensity equation (TIE) approach, where the phase intensity distribution is mathematically retrieved from multiple bright-field images with different focal planes.[27] QPI was performed on an Olympus IX-70 microscope using Kohler illumination filtered at 590 nm (FWHM = 10 nm; Thorlabs), and bright-field images were collected using a 40X 0.75 NA air objective (Olympus). Images were acquired using a 12-bit, 2048 pixel x 2048 pixel, Retiga 4000 CCD camera (Qimaging, Surrey, Canada) and collected with Micro-Manager (www.micro-manger.org) open source microscopy software. Multiple bright-field images at differing focal planes were obtained by manual turning the z-direction optical focus (1 µm gradations) in 5 µm increments. The phase image was extracted and the index of refraction of the material was determined from the bright-field images using the TIE method described elsewhere[27, 28] and implemented from custom software.[29]

III. RESULTS

A. Evaluation of the SPR angle scans in the BFP imaging plane

The SPRI microscope system has been described previously[16] and is shown here schematically (Fig. 1a). Briefly, a high numerical aperture (NA) objective lens is used to direct and collect the incident and reflected light similar to the way an SPR coupling prism is used,[30] except that a range of incident angles are provided simultaneously through the objective lens. The excitation source is a digital light projector

(DLP) that provides a broad spectrum of incident light that can be selectively patterned to illuminate only a specified range of incident angles. A collection lens is used to direct the image of either the sample plane or back focal plane (BFP) onto the charged-coupled device (CCD) camera.

The light reflected from the sample that is imaged onto the BFP of the objective lens allows for construction of the angle-dependent SPR reflectivity profile of the sample. As shown in Figure 1b, the radial distance, d, of light from the center of the BFP image corresponds to the angle, θ, with which incident light impinges on the sample on the microscope stage; this is calculated according to the Abbe sine condition for a thick lens, where $d = A \sin(\theta)$ (Supplementary Material, Fig. S1).[19] While the use of an objective lens provides the great advantage of allowing analysis of reflectivity from sample at a range of incident angles, aberrations in the objective lens require compensation before the Fresnel optical model can be used accurately to fit the reflectivity/angle relationship. This is because of the attenuation of the light near the periphery of the high NA objective, which results in the uneven attenuation in the intensity of the p- and s-polarized light. Shown in Figure 1c is the SPR reflectivity profile presented as p-polarized divided by s-polarized (p/s) intensities as a function of incident angle (black line). Performing a ratio of p and s intensities has been previously shown to provide a normalized reflectivity response,[12] but in this case the reflectivity response shows an angle dependent aberration due to diattenuation[20] of the p- and s-polarized light, which requires further consideration. This polarization apodization function of the objective was measured using the reflectivity profile of a thick gold sample (no SPR response) and presented as a p/s ratio depicting the angle dependent change in intensity between p- and s-polarized light (Fig. 1c, blue line). Dividing the SPR reflectivity profile by the objective apodization function results in a normalized SPR reflectivity profile (green line) that can now be fit with a Fresnel model (magenta line) using published values for the prism/gold/water interface.[21-23] The index of refraction for water (n = 1.333 at 590 nm) is used to calibrate the distance-angle relationship for this microscope system. A step-by step description of the normalization of the SPR angle analysis through a high numerical aperture microscope objective is shown in Supplementary Material Figure S2, and described in Materials and Methods.

B. Validation of the index of refraction values generated by SPR angle scans and imaging

To demonstrate that the apodization correction makes it possible to accurately measure index of refraction using SPR and a high NA objective, we validated the system calibration with bulk materials of known or independently measured index of refraction values. Images of the BFP for water, PBS buffer, ethanol and polymerized PDMS samples are shown in Figure 2a showing that the angles of minimum reflectance vary. The image data are plotted as corrected angle-dependent SPR intensity curves (Fig. 2b), and the Fresnel model results for the index of refraction values (Table I), are in agreement with index of refraction values observed by critical angle measurements (Supplementary Material, Fig. S3). This indicates that the apodization correction allows reflectivity data obtained from the BFP to be fit by the Fresnel equations to generate accurate index of refraction values. Also, the shift in SPR angle minimum, $\Delta\theta_{min}$, for each material is plotted versus its index of refraction as measured by critical angle, or as reported in the literature, and overlaid with a Fresnel model simulation (Fig. 2c) to show the linear relationship between $\Delta\theta_{min}$ and index of refraction in agreement with theory.[30]

For achieving an SPR image of a sample, incident light at a single angle is projected on the BFP and the image plane is visualized. This is achieved by generating a crescent shaped illumination band using the DLP and spatially positioning it on the BFP to correspond to a single angle of incidence (Fig. 2d). We chose 56.5° as depicted by the green line in Figure 2b, because this incident angle is lower than the resonance minimum and that the reflectivity intensity will increase as index of refraction values increase. The resulting SPR images are shown in Figure 2e for each bulk material, reported as ΔR reflectivity, in which the reflectivity values are normalized to the water sample. Since these are homogeneous bulk samples, there are no image features to be observed; however, we show these images to indicate the homogeneity of the samples and the differences in their reflectivity values. These ΔR values are plotted as a function of the index of refraction for each material and this plot is overlaid with a Fresnel model simulation of ΔR values versus index of refraction extracted from SPR reflectivity calculations for an incident angle of 56.5° (Fig. 2f). This shows that the relationship between SPRI reflectivity and index of

refraction may be non-linear depending on the magnitude of the differences and the angle of reflectance that is used for normalization. Thus, this method is important for determining the dynamic ranges of an imaging system. Additionally, the measurement error in index of refraction for the materials in both Figure 2c and 2f (x-axis error, $\sigma \approx 0.001$) are similar and small except for that derived from the reflectivity measurement of PDMS in Figure 2f (x-axis error, $\sigma = 0.010$). This indicates that at large change in reflectivity (e.g. $\Delta R = 0.59$) and a small amount of measurement error in reflectivity translates into about 10x the error in determining the index of refraction than if the same magnitude of error occurred at a lower reflectivity value (e.g. $\Delta R = 0.40$).

C. SPRI measured index of refraction for polymer microspheres

We investigated the ability to measure the SPRI reflectivity for several polymer microspheres in water to determine index of refraction values based upon the system calibration used to convert reflectivity values into index of refraction values. Figure 3a shows bright field and SPR images of several microspheres of different sizes and composition, namely gelatin impregnated in 4% agarose, Sephacryl, and silica. Sephacryl is the trade-name for a covalently cross-linked allyl dextrose gel formed into beads. While the transmission-mode bright field images depict each microspheres' entire diameter, the SPR images show only the portion of the bead that is within the detectable limit of the evanescent wave penetration depth, as described previously.[16] We are interested in measuring the maximum reflectivity for each of the microsphere materials relative to water (ΔR); we do this by determining reflectivity across the center of the bead (Fig. 3b) where the mass of material, and therefore the reflectivity, is greatest and where there is minimal contribution from surrounding media. The average ΔR_{max} values are reported (Fig. 3c) for a selection of polymer microsphere materials, each of which have distinct ΔR_{max} values but similar standard deviations in measurement error. By plotting the ΔR_{max} values of the microspheres overlaid on the previous plot transforming ΔR values into index of refraction (Fig. 3d), we can determine the index of refraction for the hydrated gelatin, Sephacryl, and silica, microspheres. As shown for the PDMS material (Figure 2e), the silica microsphere has a large ΔR_{max} value which propagates the small measurement error into a much

larger uncertainty error in the index of refraction value when compared to that calculated for the gelatin or Sephacryl microspheres. The PMMA material showed the largest ΔR_{max} value (displayed only in Figure 3c), however, the magnitude was large enough to be effectively off-scale and cannot be accurately converted into index of refraction with the current experimental conditions.

The index of refraction measurements for the polymer microspheres were independently measured with quantitative phase imaging (QPI), using bright field imaging and transport of intensity equations (Supplementary Material, Fig. S4).[27, 31] These index of refraction measurements along with those measured by SPRI and literature reported values[32] are reported in Table II. The comparison of index of refraction values between QPI and SPRI shows good agreement within the error of measurement. We are unaware of published values for refractive index of hydrated gelatin or Sephacryl microspheres.

IV. DISCUSSION

A. SPR polarization apodization correction

It has been shown that in prism-based SPRI, dividing the p- polarized image by the s- polarized image improves image quality in two ways. First, it effectively increases the spatial homogeneity of the incoming illumination, and second it allows ratiometric normalization of the reflectivity intensity values.[12] In a similar manner, when using a high NA objective for SPRI, the procedure has been shown to improve image quality.[16] However, due to the diattenuation observed at the steep angles in a high numerical aperture objective, an additional procedure is required to measure the apodization function and perform a mathematical correction to accurately normalize the SPR reflectivity response. This correction is critical to successfully model the reflectivity curve with the Fresnel equations to extract accurate optical parameters. While we have performed a mathematical correction here, there are optical methods described to rectify the differential attenuation, and this is a strategy that may be evaluated in the future.[19]

Other strategies to correct for diattenuation are to only use the p-polarized SPR scan or image and either use only a p-polarized attenuation function or simply normalize to arbitrary reflectivity units. These simple conversions appear more straight-forward, but the images show larger background noise and are more sensitive to the quality and spatial homogeneity of the incoming illumination (data not shown). Retaining the apodization function as a p/s intensity ratio as demonstrated here improves these aspects of the image data and appears to be fairly robust to minor changes in optical alignment.

B. SPR and SPRI index of refraction measurements

The bulk materials selected for SPR index of refraction measurements were selected to contain a wide range of index of refraction values that are biologically relevant. They are homogeneous materials with no specific features (Fig. 2e) so that measurements from the SPR angle scan in the BFP can be readily compared with SPRI measurements from the image plane. The reflectivity values in the image can be averaged across the whole image and the averaged value directly compared to the reflectivity value of the selected SPR angle in the BFP. This methodology facilitates the application of the SPR angle scan in the BFP to aid with SPRI set-up, calibration, and quantitation.

When performing SPR imaging at a fixed angle, the reflectivity to index of refraction relationship will have both near linear and nonlinear regions, the extent of which is highly system dependent. This response has been observed here using the measurement of selected materials, and also by simulation with Fresnel theory (Fig. 2f). It is important to characterize and understand the ranges of linear and nonlinear response. Operating within the linear response range allows for straightforward downstream analysis where errors in the measured index of refraction values are small. The system described here has an approximately linear response in the ΔR range below ≈ 0.4. This is likely to be ideal for many biologically relevant measurements in aqueous media, since all of the time-dependent reflectivity measurements we have made thus far using SPRI on single cells and extracellular matrix, have had measured ΔR values < 0.3.[12, 13, 16] Assuring that measurements are in the linear range facilitates conversion of reflectivity units into index of refraction and other derived units such as mass of material deposited at the surface.

As shown in the right-hand scale of Figure 2c, the $\Delta\theta_{min}$ SPR response remains entirely linear across large refractive index changes, as expected and corroborated by theory.[33] If it becomes important to accurately measure index of refraction across a wide dynamic range, an experimental method to collect SPR images from multiple incident angles can be designed, and from that series of images acquired with different incident light angles, a composite image of $\Delta\theta_{min}$ or index of refraction values can be determined.

C. SPR image intensity analysis of polymer microspheres

In previous work with polymer microspheres of various index of refraction values, we have reported limits of detection associated with the SPR penetration depth[16] which were similar for all measured microspheres. From this current study we conclude that the SPRI measured ΔR values for many of those microspheres were large and in the non-linear response range close to the SPRI signal saturation. Only two of the polymer microsphere materials measured here, the hydrated 4% agarose with gelatin bead and the hydrated Sephacryl bead, are distinctly within the linear response range and can be reliably converted to an index of refraction value with minimal error using the calibration process and optical models.

As shown in Table II, the solid materials (silica and PMMA) have index of refraction values larger than $n = 1.42$. These materials are less accurately measured by SPRI under the conditions used in this study. However, an accurate measurement of Sephacryl, which has not been previously optically characterized, can be made by SPRI, and indicates an index of refraction value that is lower than most solid polymer microspheres. It is presumed that these microsphere materials do not have a reported refractive index value because they are highly porous and therefore the overall index of refraction for the microsphere will be highly dependent on the solvent they are suspended in. Despite this, the Sephacryl microsphere in aqueous media, which has a ΔR value of 0.357 and index of refraction value of 1.358, maybe able to serve as suitable SPRI benchmark artifact that can be used as both an intensity benchmark, having similar ΔR values to that of cells, as well as a measurement tool to detect the SPR penetration depth, as described previously.[16]

Identifying materials that mimic the optical properties of biological samples is important for the purpose of calibrating and optimizing SPRI as well as other measurement techniques sensitive to optical properties, such as quantitative phase imaging. In this study, the use of SPRI allowed a simple measurement of index of refraction for low index of refraction materials in aqueous solutions. This strategy may be useful for identifying and generating new reference materials that can be used to calibrate optical detection methods including and beyond SPRI to facilitate the use of these techniques as quantitative tools for probing biological systems. Because the SPR microscope system described here can be adapted to existing microscopes in many laboratories, the identification and use of calibration materials will enable data comparability between the laboratories.

V. CONCLUSION

Previously, we demonstrated that a high NA microscope objective for SPR imaging can be used to achieve near-diffraction-limited spatial resolution and to measure sub-cellular features including focal adhesions.[16] Here we aid the quantitative interpretation of the reflectivity intensity values with an objective-specific apodization correction, calibration materials with indices of refractions close to biological cells, and a validation strategy along with supporting optical modeling. The SPR microscope provides measurements of the sample in both the back focal plane (to provide angle-dependent reflectivity data) and in the imaging plane (to provide pixel-level image data at a single optimized angle of incidence). We show how to correlate the distance-dependent data from the BFP with the SPRI reflectivity intensities at the selected angles of illumination. A variety of polymer microspheres were assessed as potential intensity calibrants by measuring their range of reflectivity and index of refraction values. A comparatively low refractive index material, such as hydrated Sephacryl microspheres, seems to be ideally suited as an intensity benchmark material. This material has a reflectivity that is similar in magnitude to that of cells, extracellular matrix, and other biological materials. Taken together, this work provides a framework to extract accurate, quantitative optical parameters from biological specimens such as cells, sub-cellular

features, and extracellular deposited materials, with the use of material, models and procedures for benchmarking, calibrating and determining the dynamic range of an SPR microscope imaging system.

VI. FIGURES

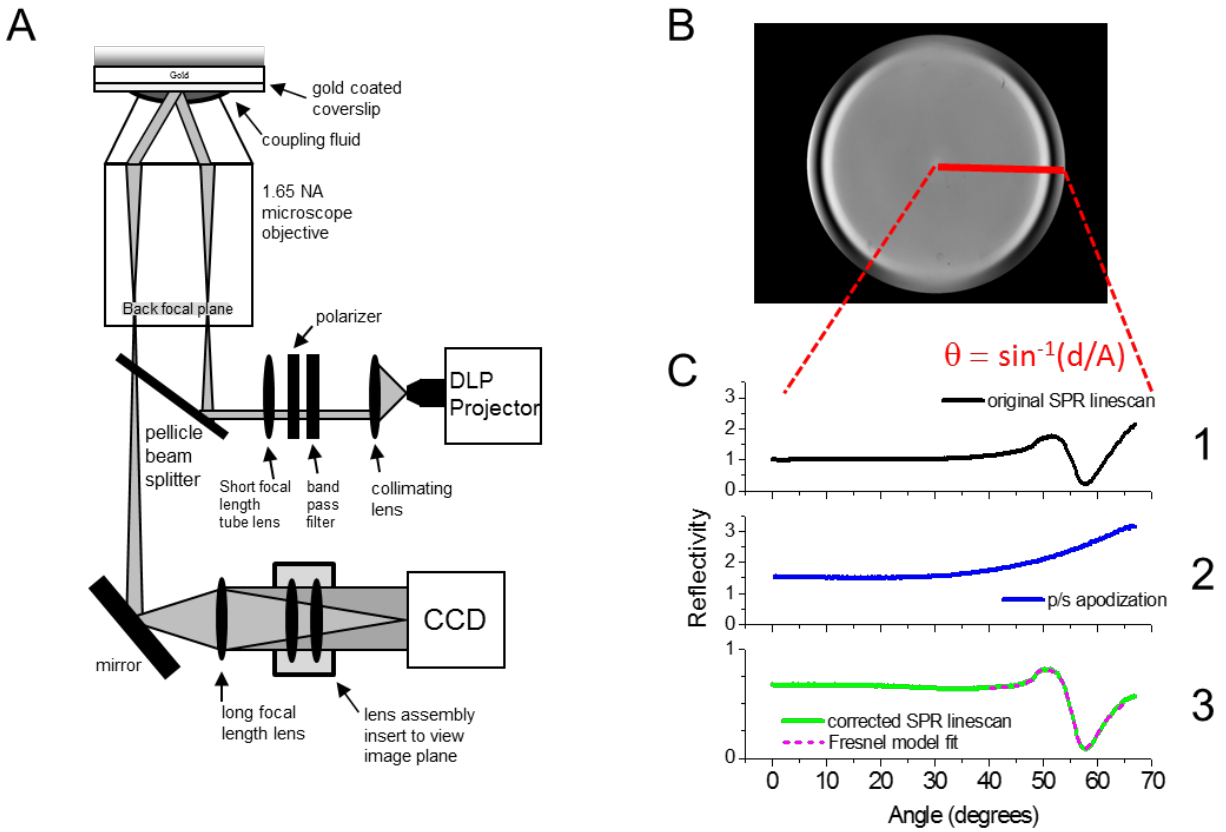

FIG. 1. Instrument schematic for SPR imaging using a high NA objective and imaging of the back focal plane (BFP). A) A digital light projector generates and patterns light to control the angle of incident light, which is collimated, wavelength selected, linearly polarized, and directed through an inverted microscope platform. The image that is reflected from the sample is captured on a CCD camera. A movable lens assembly before the CCD camera selects for either the image plane or BFP. B) The image in the BFP formed by light reflected from a sample of water that is fully illuminated with 590 nm light linearly polarized in the x-direction and collected with the objective lens in optical contact with a coverslip coated with a 45 nm film of gold under water. The darkest crescent shaped regions indicate the angle at which the p-polarized incident light maximally couples to surface plasmons. P-polarized light couples maximally at high incident angle in the *x*-axis, and not in the *y*-axis where the light is s-polarized. The red line depicts the angular distribution of incident light onto the image plane from the center of the BFP (0°) to the periphery (≈ 68° – based upon SPR data fitting). C) The angle dependence of the p-polarized divided by the s-polarized light intensities from the line scan shown in B) converted from a distance measurement to an angle of incidence according to equation shown. The uncorrected SPR angle scan (C1 - black line) shows an angular dependent distortion in reflectivity values due to objective aberrations at high NA angles. The objective apodization is measured by using a p/s line scan of a reflective thick gold sample (C2). The original SPR data divided by the apodization function results in a normalized SPR angle scan (green line) that can be modeled and fit with the Fresnel optical model using literature values for a glass/gold/water layer interface (magenta line) (C3).

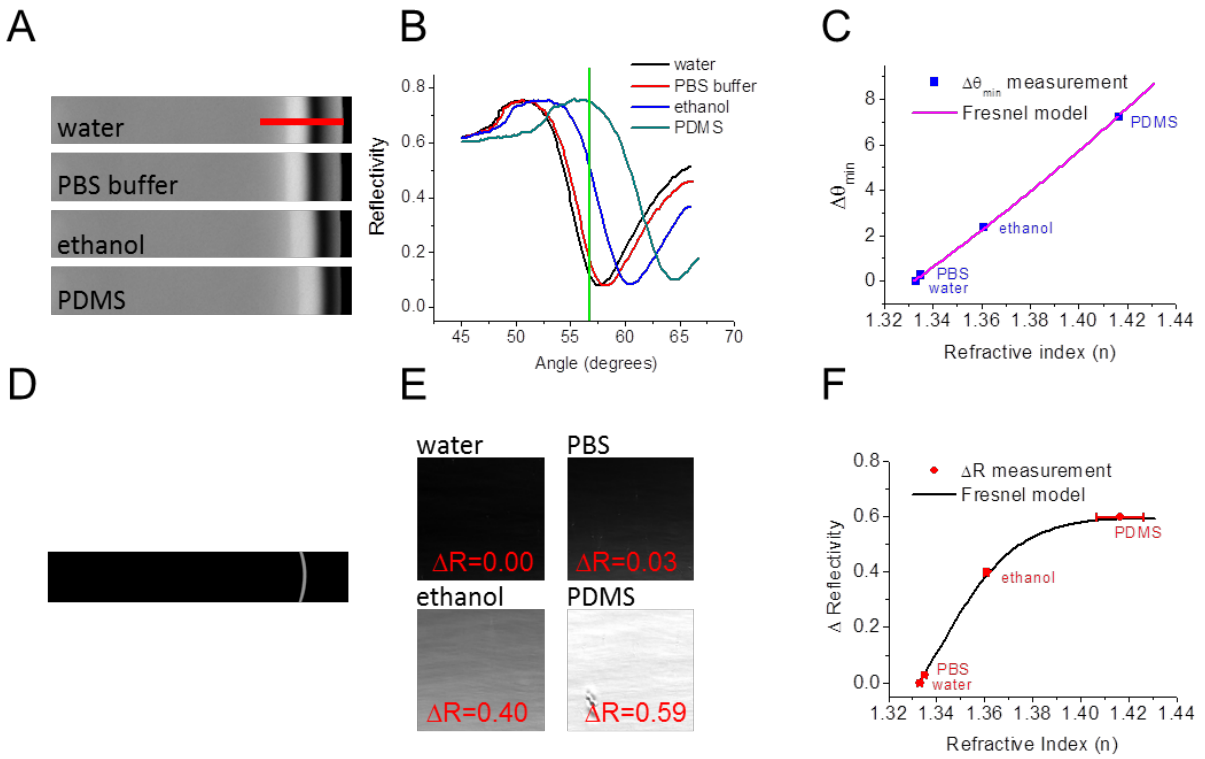

FIG. 2. Four bulk materials with different values of index of refraction are measured by SPR with a range incident angles through the high NA objective lens; the fully illuminated sample is imaged in the BFP. A) Select region of the BFP images for each of the 4 different index of refraction materials, water, phosphate buffered saline (PBS), ethanol, polydimethylsiloxane (PDMS), which shows an illumination angle range of 0° to 68° of 590 nm linearly p-polarized light The dark region (indicating minimum reflectivity) of the SPR reflectance can be seen to incrementally shift towards the periphery of the BFP, corresponding to a shift in the angle of maximum coupling to surface plasmons. The red line corresponds to an approximate angle range of 45° to 68°. B) Reflectivity as a function of angle of incidence of illumination for each material in A) shows a shift in the SPR minimum observed that increases with increasing refractive index of the material: water (n = 1.333), PBS buffer (n = 1.335), ethanol (n = 1.362), and PDMS (n = 1.416). The green line in the plot highlights the angle of incidence for 56.5°. C) Plotted is the SPR reflectivity minimum (θ_{min}) interpreted from B) (blue squares) along with a Fresnel model of θ_{min} shift (magenta line) that shows a direct linear relationship of θ_{min} with refractive index change. D) Instead of fully illuminating the sample as in A), this BFP image shows the digitally patterned incident angle illumination at 56.5° used for subsequent SPR imaging. E) SPR images of the above materials measured using the 56.5° incident angle illumination pattern shown in D) and depicted in B). The images are displayed in ΔR intensity values normalized to water. The raw reflectivity intensity of water is ≈ 0.1. F) Average ΔR values from E) are plotted versus the measured refractive index values for water, PBS, ethanol, and PDMS (red circles). Overlaid, is a 3-layer Fresnel model of ΔR shift (black line), generated for 56.5° with the refractive index of the media layer varied from 1.333 to 1.420, and ΔR intensity values normalized to water. The ΔR response becomes nonlinear for large changes in refractive index.

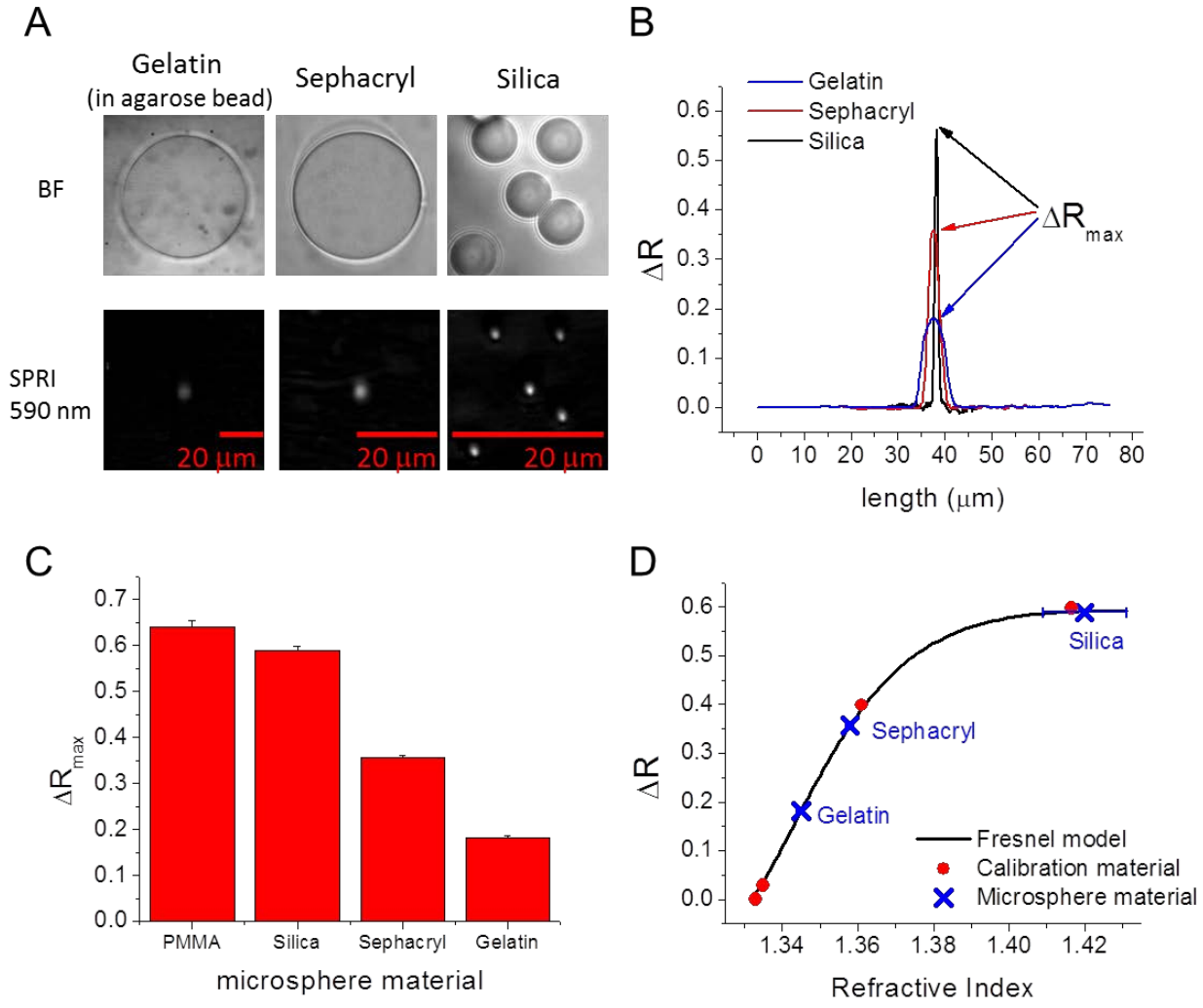

FIG. 3. Maximum values of ΔR determined from SPRI for several polymer microspheres and conversion to index of refraction values. A) Bright field and SPR images of a gelatin-coated 4% agarose, Sephacryl, and silica microspheres, each in water. Scale bars of 20 µm apply to both bright field and SPR images. B) Line scans (not displayed on image) through the center of beads in each SPR image in A) where the indicated ΔR_{max} is the maximum ΔR intensity due to plasmon resonance coupling for each type of microsphere. C) Average ΔR_{max} values plotted as a function of bead materials. Standard deviations show the average value for ≥ 6 beads. D) Plot of the ΔR_{max} values for microspheres from C) onto the plot of ΔR values versus index of refraction for the bulk materials and Fresnel model discussed in Fig. 2f. From this plot, predicted values for refractive index of the microspheres can be determined. Only the microsphere materials with index of refraction values lower than silica (n = 1.42) are accurate, and so PMMA is not displayed.

VII. TABLES

Table I. Refractive index values of bulk optical reference materials used in this study. The water refractive index value is a reference valued used for system calibration. The other material refractive index values are the results of the Fresnel model. Error reported as standard deviation.

Sample	**Critical Angle: Index of Refraction**	**SPR: Index of Refraction**
Water	1.3330	1.3330
PBS buffer	1.3349 ± 0.0001	1.3351 ± 0.001
Ethanol	1.3609 ± 0.0004	1.3617 ± 0.001
PDMS	1.4165 ± 0.0001	1.4161 ± 0.001

Table II. Comparison of literature reported values for index of refraction of select polymer microspheres alongside with SPRI and QPI measured values with associated standard deviations in measurement. (xx = no data or citation available).

Microsphere Material	*n* (reported)	SPRI *n* (measured)	QPI *n* (measured)
PMMA	1.484[32]	xx	1.481 ± 0.001
Silica	1.421[32]	1.420 ± 0.011	1.425 ± 0.003
Sephacryl	xx	1.358 ± 0.001	1.359 ± 0.004
Gelatin (4% agarose bead)	xx	1.345 ± 0.001	1.344 ± 0.002

SUPPLEMENTARY MATERIAL

See supplementary material for supplementary figures S1 – S4.

REFERENCES

1. J. Homola, *Surface plasmon resonance based sensors*. (Springer, 2006).
2. M. Gotoh, Y. Hasegawa, Y. Shinohara, M. Shimizu and M. Tosu, DNA Res. **2** (6), 285-293 (1995).
3. D. Altschuh, M. C. Dubs, E. Weiss, G. Zederlutz and M. H. V. Vanregenmortel, Biochemistry **31** (27), 6298-6304 (1992).
4. K. A. Peterlinz and R. Georgiadis, Langmuir **12** (20), 4731-4740 (1996).
5. H. H. Nguyen, J. Park, S. Kang and M. Kim, Sensors **15** (5), 10481-10510 (2015).
6. W. Wang, S. Wang, Q. Liu, J. Wu and N. Tao, Langmuir **28** (37), 13373-13379 (2012).
7. C. L. Wong and M. Olivo, Plasmonics **9** (4), 809-824 (2014).
8. A. Zybin, Y. A. Kuritsyn, E. L. Gurevich, V. V. Temchura, K. Uberla and K. Niemax, Plasmonics **5** (1), 31-35 (2010).
9. L. K. Wolf, D. E. Fullenkamp and R. M. Georgiadis, J Am Chem Soc **127** (49), 17453-17459 (2005).
10. B. P. Nelson, T. E. Grimsrud, M. R. Liles, R. M. Goodman and R. M. Corn, Analytical chemistry **73** (1), 1-7 (2001).
11. G. J. Wegner, N. J. Lee, G. Marriott and R. M. Corn, Analytical chemistry **75** (18), 4740-4746 (2003).
12. A. W. Peterson, M. Halter, A. Tona, K. Bhadriraju and A. L. Plant, BMC cell biology **10**, 16 (2009).
13. A. W. Peterson, M. Halter, A. Tona, K. Bhadriraju and A. L. Plant, Cytom Part A **77A** (9), 895-903 (2010).
14. B. Huang, F. Yu and R. N. Zare, Analytical chemistry **79** (7), 2979-2983 (2007).
15. S. Wang, X. Shan, U. Patel, X. Huang, J. Lu, J. Li and N. Tao, Proceedings of the National Academy of Sciences **107** (37), 16028-16032 (2010).
16. A. W. Peterson, M. Halter, A. Tona and A. L. Plant, BMC cell biology **15**, 35 (2014).
17. Certain commercial equipment, instruments, or materials are identified in this paper in order to specify the experimental procedure adequately. Such identification is not intended to imply recommendation or endorsement by the National Institute of Standards and Technology, nor is it intended to imply that the materials or equipment identified are necessarily the best available for the purpose.
18. E. Hecht, *Optics*. (Addison-Wesley Longman, Inc., Reading, MA, 2002).
19. P. Torok and F.-J. Kao, *Optical imaging and microscopy*. (Springer-Verlag, Berlin, 2003).
20. M. Shribak, S. Inoue and R. Oldenbourg, Optical Engineering **41** (5), 943-954 (2002).
21. Schott North America, Advanced Optics, Abbe diagramm, URL: http://www.us.schott.com/advanced_optics/english/knowledge-center/technical-articles-and-tools/abbe-diagramm.html.
22. G. M. Hale and M. R. Querry, Applied Optics **12** (3), 555-563 (1973).
23. E. D. Palik, Handbook of Optical Constants of Solids, (Academic Press, Inc., Orlando, 1985), pp. 804.
24. J. S. Shumaker-Parry and C. T. Campbell, Analytical chemistry **76** (4), 907-917 (2004).
25. T. A. Morris, A. W. Peterson and M. J. Tarlov, Analytical chemistry **81** (13), 5413-5420 (2009).
26. J. H. Grassi and R. M. Georgiadis, Analytical chemistry **71** (19), 4392-4396 (1999).
27. D. Paganin and K. A. Nugent, Phys Rev Lett **80** (12), 2586-2589 (1998).

28. M. Mir, B. Bhaduri, R. Wang, R. Y. Zhu and G. Popescu, Prog Optics **57**, 133-217 (2012).
29. D. C. Ripple and Z. Hu, Pharmaceutical research (2016).
30. H. Raether, *Surface Plasmons on Smooth and Rough Surfaces and on Gratings*. (Springer-Verlag, Berlin, 1988).
31. C. J. Bellair, C. L. Curl, B. E. Allman, P. J. Harris, A. Roberts, L. M. D. Delbridge and K. A. Nugent, J Microsc-Oxford **214**, 62-69 (2004).
32. Z. S. Hu and D. C. Ripple, J Res Natl Inst Stan **119**, 674-682 (2015).
33. E. Stenberg, B. Persson, H. Roos and C. Urbaniczky, J Colloid Interf Sci **143** (2), 513-526 (1991).

SUPPLEMENTARY MATERIAL

Surface plasmon resonance microscopy: achieving a quantitative optical response

Alexander W. Peterson, Michael Halter, Anne L. Plant, and John T. Elliott

Biosystems and Biomaterials Division, National Institute of Standards and Technology, 100 Bureau Dr., Gaithersburg, MD 20899, USA

CONTENTS:

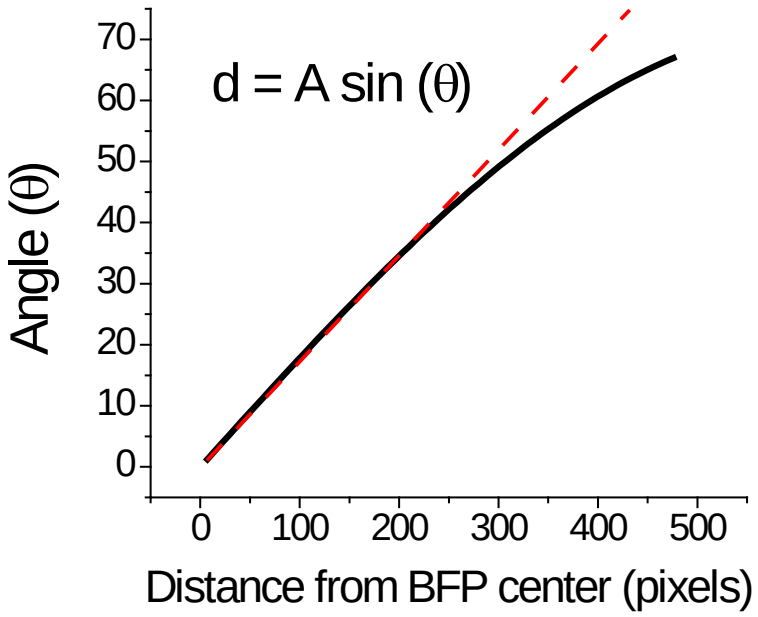

FIG. S1. Back focal plane distance to incident angle conversion. The angle of incident light on the sample plane (θ) is related to position on the back focal plane (*d*) according to the Abbe sine condition shown here as $d = A \sin(\theta)$. *d* is measured as distance from the center of the back focal plane as measured in pixels. A is a constant that is determined from a known θ and measured *d*. Here we use the critical angle of water, $n = 1.333$ for $\lambda = 590$ nm, of $\theta = 48.3°$, for $n = 1.78$. Alternatively, one can use the measured distance from the center to the periphery of the back focal plane calculated to be $\theta = 68.0°$ based upon the numerical aperture of the objective (NA = 1.65) with $n = 1.33$ according to the relation, $NA = n \sin(\theta)$. In the graph above, one can qualitatively observe the distance versus angle relationship as fairly linear until the larger angles of incidence. A straight line (red dashed) is shown for comparison. However, the nonlinear curvature occurs right at the high angles of incidence where the SPR measurements take place, therefore it is important to implement this conversion above instead of a linear approximation to obtain accurate θ values.

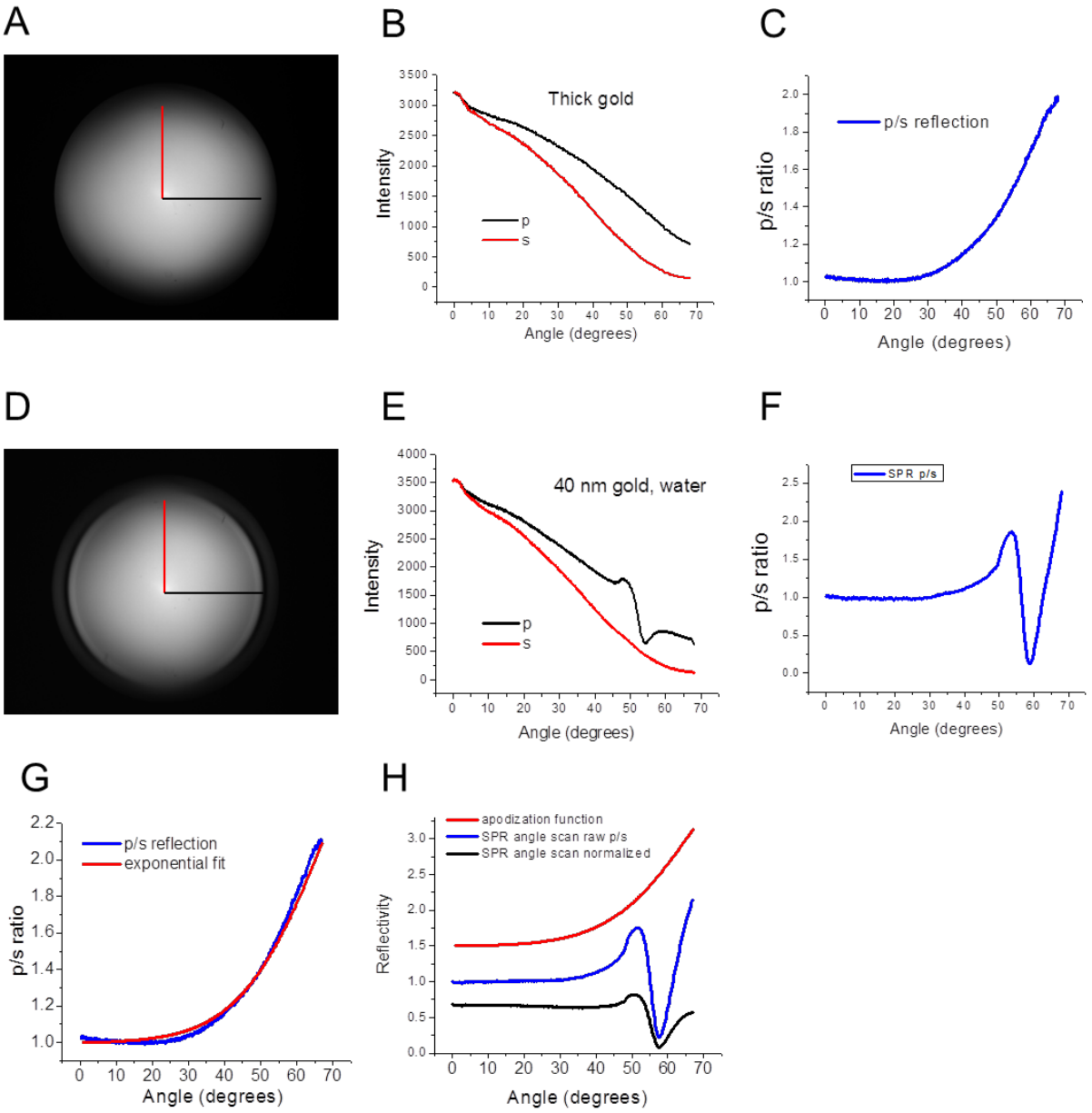

FIG. S2. Accounting for the differential transmission between p- and s-polarization through a high numerical aperture objective. A) Image of reflected light, at the back focal plane (BFP) of a 1.65 NA objective at 590 nm, off a thick gold sample, with linear polarization along the horizontal axis. A line scan from center of BFP to periphery is displayed in black for the p-polarized direction and in red for the s-polarized direction. B) The intensity of the p- and s-polarized lines scans are plotted as a function of incident angle after conversion from distance units from center to periphery of the BFP. The difference in intensity values depicts the differential transmission between p- and s-polarized light through a 1.65 NA objective. C) By dividing the p- by s-polarized light intensity values the resulting plot shows the apodization effect as a ratio of p/s light intensity and the ratio increases near the periphery of the high numerical objective. D) The same image condition as A) except the sample is a thin gold (40 nm) under water media, allowing for generation of surface plasmon resonance (SPR) at the BFP periphery. E) Same type of line scan plot as in B) except in addition to displaying the differential transmission of p- and s-polarized light, one can also observe the surface plasmon resonance in the p-polarized light. F) Similar plot as in C) except now one can

observe both the apodization of p/s light from the high NA objective as well as the surface plasmon resonance. G) The p/s reflection ratio in C) can be fit to an exponential function, of the form $Ae^{(x/c)} + y_1$, as shown by the red line, where x is the angle in degrees and the other values are fitted constants (A, c, and y_1). The overall magnitude of the function can be adjusted by the y_1 value such that dividing by this apodization function will normalize the SPR angle scan into appropriate reflectivity units. H) By dividing the raw SPR angle scan in F) (blue line) by the adjusted apodization function obtained in G) (red line) the resulting SPR curve (black line) is now corrected for the differential transmission of p- and s-polarized light in the high numerical objective and is appropriately normalized, and can be fit and modeled by the Fresnel model as typically used for SPR in the typical Kretschmann configuration.

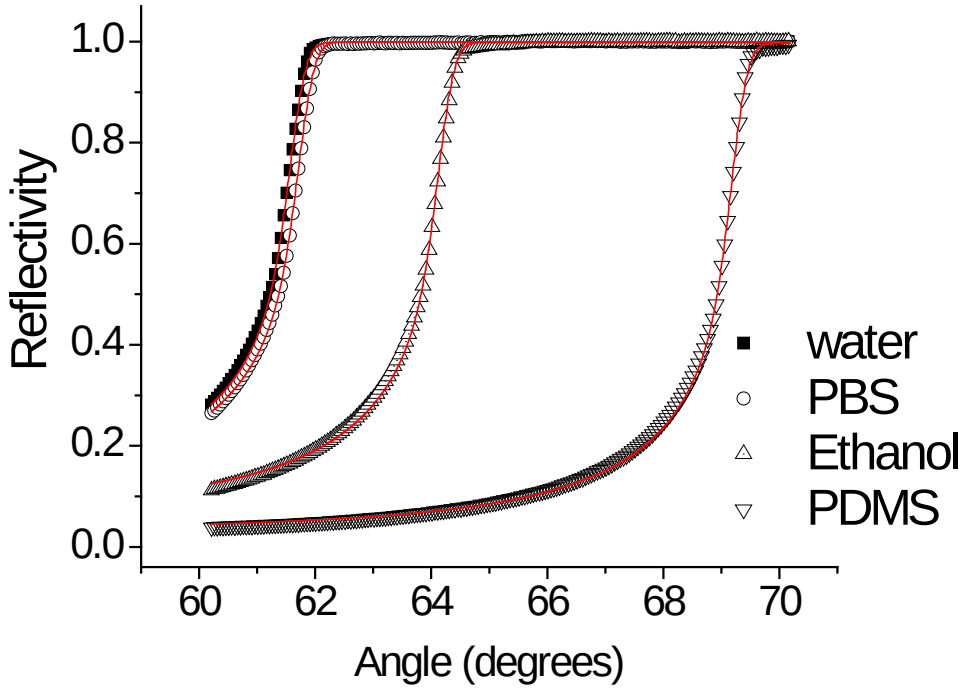

FIG. S3. Critical angle data to validate reference materials. Reflectivity data as a function of angle of incidence for λ = 590 nm near the critical angle for water (squares), PBS buffer media (circles), ethanol (up-triangle), and PDMS (down-triangle). Overlaid on each data set are fits to the two-layer Fresnel model to measure the bulk material refractive index. The angle of incidence value is initially calibrated to the refractive index reference value for water. The model determined refractive index for each material is reported in Table I.

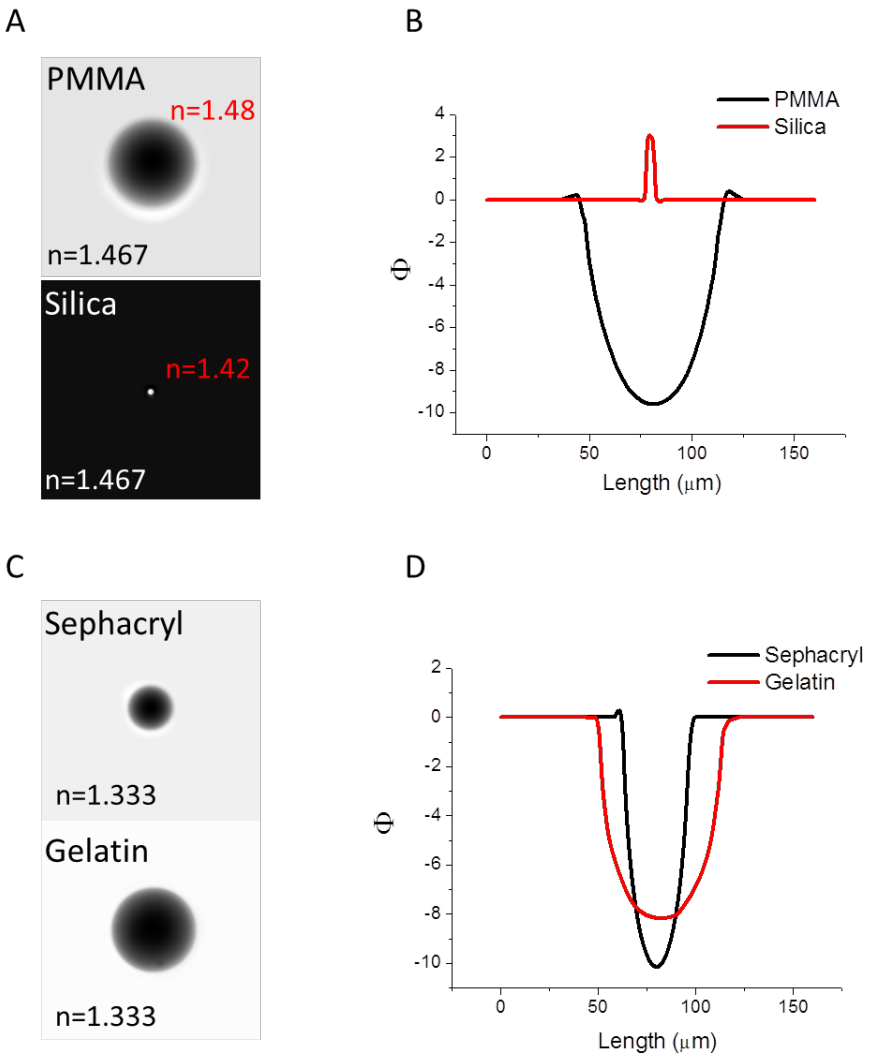

FIG. S4. Quantitative phase imaging to measure refractive index of polymer microspheres. A) The optical phase was imaged for two types of polymer microspheres with known refractive index values, known refractive index of media (mineral oil, n = 1.467), and known dimensions, using the transport of intensity equation which generates a spatial phase distribution by mathematical manipulation of multiple bright field images with different focal planes. B) The cross section of $\boldsymbol{\phi}$ values through each microsphere is displayed. From the maximum $\boldsymbol{\phi}$ value at the center of the microsphere, the refractive index can be calculated by solving this equation $\boldsymbol{\phi = 2\pi/\lambda(n_1-n_2)t,}$ where λ is wavelength used (0.59 μm), $\mathbf{n_1-n_2}$ is the difference in refractive index for the media minus the microsphere, and **t** is the thickness, or diameter, of the microsphere. The measured refractive index values for these two microspheres agree with the reported values within the error of 5 measurements (Table II in manuscript), and serve as validation of the technique methodology. C) The optical phase was imaged two types of polymer microspheres with unknown refractive index, known refractive index of media (water, n =1.333), and experimentally measured dimensions. D) Using the maximum absolute value of $\boldsymbol{\phi}$ measured from the plotted cross sections through the center of the microspheres, the refractive index was calculated based on the formula above. The index of refraction values for these microspheres are compared (in Table II of manuscript) with the index of refraction values obtained from surface plasmon resonance imaging to validate the values measured from close surface contact.